Supporting Information

Two binuclear Ni-inserted polyoxotantalates based on $\{NiTa_{10}O_{32}\}$ units with catalytic activity

Hui Zhao, Hanhan Chen, Mingyang Zhang, YuanyuanYang, Zongfei Yang, Pengtao Ma, Jingyang Niu* and Jingping Wang*

Henan Key Laboratory of Polyoxometalate Chemistry, College of Chemistry and Molecular Sciences, Henan University, Kaifeng Henan 475004 (P.R. China)

Corresponding Author

E-mail address: jyniu@henu.edu.cn (J. Niu), jpwang@henu.edu.cn (J. Wang)

Contents

Section 1 Experimental section

1.1 Materials and methods

$K_8Ta_6O_{19}\cdot 17H_2O$ was prepared using literature methods and characterized by IR spectrum.[1] The others were obtained from commercial sources. The IR spectra were obtained by using a Bruker Vertex 70 IR spectrometer using KBr pellets. Thermogravimetric analyses (TGA) of these compounds were performed using a Mettler-Toledo TGA/SDTA 851e instrument under an N_2 atmosphere. XRPD data were collected on a Bruker AXS D8 Advance diffractometer instrument with Cu Kα radiation at 293 K. Magnetic properties of compounds **1** and **2** were investigated on a Quantum Design SQUID MPMS3 magnetometer. All electrospray-ionization mass spectrometry (ESI-MS) measurements were performed on an AB SCIEX Triple TOF 4600 spectrometer operating in negative ion mode and the data were analyzed using the Peakview 2.0 software. Proton conductivity measurements were tested using Solartron 1260 and 1296 impedance phase gain analyzers, and the scanning frequencies ranged from 10 MHz to 0.01 Hz with a voltage of 0.1 V. the mixture was qualitatively analyzed by GC-MS (Agilent 7890B GC/5977B MS) and quantitatively analyzed by a gas chromatograph (Bruker 450-GC flame ionization detector) instrument equipped with a 30 m column (GsBP-5, 0.25 mm internal diameter and 0.25 μm film thickness) with nitrogen as a carrier gas.

1.2 X-ray crystallography

The crystals of **1** and **2** were selected and the structural measurements were performed at 150 K on a Bruker Apex-II CCD diffractometer using graphite-monochromated Mo Kα radiation (λ = 0.71073 Å). After data collection, Dates reduction, including a correction for routine Lorentz and polarization, was performed by an applied multiscan absorption correction SADABS program. The crystal structures were solved by the direct method and refined by full matrix least-squares on all F^2 data using the SHELX program suite.[2] The remaining lattice water molecules were determined by TGA results. CCDC numbers are **2202094** (**1**) and **2202093** (**2**) Crystal dates and structure refinements are provided in Table S1.

1.3 Synthetic

Synthesis of **1**: A mixture of $K_8Ta_6O_{19}\cdot 17H_2O$ (3g, 1.5mmol), Na_2SeO_3(0.138g, 0.75mmol) and $Ni(NO_3)_2\cdot 6H_2O$ (0.87g, 3mmol) was dissolved into 50 mL of H_2O, after stirring for 15 minutes, and 975μL 1,2-dap was added to the above solution, then the solution was kept at 160 ℃ for 3 days. The violet filtrate was transferred to a straight glass tube, and a mixed solvent of CH_3CH_2OH/H_2O (1:2, volume ratio) was carefully layered onto the filtrate. Subsequently, alcohol was carefully layered onto the mixed solvent. The blue sheet crystals of **1** were obtained after one month. Yield: 10% (based on $K_8Ta_6O_{19}\cdot 17H_2O$). Calcd (%): Ni, 3.76; Ta, 58.05. Found: Ni, 3.65; Ta, 55.07. IR (KBr pellet): 3290, 1671, 857, 735, 670, 538 cm^{-1}.

Synthesis of **2**. The synthetic methods of compounds **2** and **1** are similar, except that Na_2SeO_3(0.259g, 1.5mmol) and 1,2-dap was replaced with en (835 μL). Yield: 15% (based on

$K_8Ta_6O_{19}\cdot 17H_2O$). Calcd (%) for **2**: C 0.75, H 1.50, N 0.87; found: C 0.82, H 1.63, N 0.92. IR (KBr pellet); 3290, 1671, 1031, 863, 746, 675, 539 cm^{-1}.

Section 2 Supplementary Structural Figures and Tables

Table S1. Crystal data and structure refinement for **1** and **2**.

Compound	**1**	**2**
Formula	$H_{48.5}K_{5.5}Na_2Ni_2O_{55}Ta_{10}$	$C_2H_{48}K_6N_2Na_4Ni_2O_{54}Ta_{10}$
Formula weight	3116.73	3217.80
Temperature/K	150	150
Crystal system	monoclinic	monoclinic
Space group	*C2/m*	*C2/c*
a (Å)	20.2839(12)	43.8013(13)
b (Å)	14.1700(8)	14.1230(3)
c (Å)	27.1565(17)	20.2049(5)
α (°)	90	90
β (°)	117.159(2)	113.4290(10)
γ (°)	90	90
V (Å^3)	6944.8(7)	11468.4(5)
Z	4	8
ρ_{calc} /g/cm^{-3}	3.001	3.62
μ /mm^{-1}	16.658	20.203
F (000)	5546	11056
Crystal size/mm^3	0.22 × 0.2 × 0.05	0.04 × 0.04 × 0.02
Radiation	Mo Kα (λ = 0.71073)	Mo Kα (λ = 0.71073)
Independent reflections	6411 [R_{int} = 0.0574, R_{sigma} = 0.0596]	10200 [R_{int} = 0.0526, R_{sigma} = 0.0505]
Data/restraints/parameters	6411/108/384	10200/60/709
Goodness-of-fit on F^2	1.038	1.029
Final *R* indexes [I>=2σ (I)]	R_1= 0.0699, wR_2=0.2112	R_1= 0.0423, wR_2= 0.1091
Final *R* indexes [all data]	R_1= 0.0761, wR_2= 0.2192	R_1= 0.0645, wR_2= 0.1250

[a] $R_1=\Sigma||F_o|-|F_c||/\Sigma|F_o|$. [b] $wR_2=\{\Sigma[w(F_o^2-F_c^2)^2]/\Sigma[w(F_o^2)^2]\}^{1/2}$.

Table S2. Selected bond distances of **1a**.

Bond	Length	Bond	Length	Bond	Length
Ni1–O1	2.107(10)	Ta2–O20	2.335(16)	Ta4–O13	2.062(11)
Ni1–O8	2.042(16)	Ta2–O21	1.827(19)	Ta4–O17	1.784(14)
Ni1–O2	2.128(12)	Ta2–O6	2.019(14)	Ta5–O10	1.997(16)
Ni1–O20	2.014(17)	Ta2–O9	1.983(16)	Ta5–O12	1.995(14)
Ni2–O13	2.178(12)	Ta3–O1	2.066(11)	Ta5–O19	1.827(17)
Ni2–O18	2.039(17)	Ta3–O13	1.951(14)	Ta5–O8	2.329(15)
Ni2–O4	2.026(19)	Ta3–O15	1.791(15)	Ta6–O11	2.004(14)
Ni2–O7	2.054(19)	Ta3–O20	2.393(11)	Ta6–O12	1.992(12)
Ta1–O14	1.785(12)	Ta3–O4	2.051(10)	Ta6–O16	1.793(15)
Ta1–O2	1.987(9)	Ta3–O6	1.953(13)	Ta6–O5	1.980(10)
Ta1–O9	1.982(11)	Ta4–O10	1.951(14)		
Ta1–O3	1.992(7)	Ta4–O11	1.949(14)		

Table S3. Bond valence sum calculations of the Ta and Ni atoms in **1a**.

Atom	BVS	Atom	BVS	Atom	BVS	Atom	BVS
Ni1	1.86	Ta1	4.99	Ta3	4.91	Ta5	4.90
Ni2	1.90	Ta2	4.83	Ta4	5.03	Ta6	4.95

Table S4. Bond valence sum calculations of the oxygen atoms of **1a.**

Atom	BVS	Atom	BVS	Atom	BVS	Atom	BVS
O1	1.89	O7	1.85	O13	1.46	O19	1.31
O2	1.92	O8	1.81	O14	1.44	O20	1.82
O3	0.83	O9	1.67	O15	1.42	O21	1.29
O4	1.77	O10	1.73	O16	1.41		
O5	0.85	O11	1.72	O17	1.44		
O6	1.68	O12	1.64	O18	0.35		

Table S5. Selected bond distances of **2a**.

Bond	Length	Bond	Length	Bond	Length
Ta1–O8	1.976(9)	Ta5–O1	2.085(8)	Ta9–O6	2.011(9)
Ta1–O12	1.984(8)	Ta5–O14	1.940(9)	Ta9–O7	1.996(9)
Ta1–O14	2.000(10)	Ta5–O23	1.821(10)	Ta9–O13	1.966(9)
Ta1–O21	1.790(9)	Ta5–O24	2.393(8)	Ta9–O19	1.805(9)
Ta2–O5	2.003(8)	Ta6–O4	1.998(9)	Ta10–O1	2.053(8)
Ta2–O8	1.974(9)	Ta6–O10	1.991(8)	Ta10–O3	2.036(8)
Ta2–O20	1.793(9)	Ta6–O13	1.989(9)	Ta10–O7	1.951(9)
Ta2–O24	2.400(8)	Ta6–O17	1.806(9)	Ta10–O9	1.916(9)
Ta3–O5	1.999(8)	Ta7–O2	2.056(8)	Ni1–O1	2.108(9)
Ta3–O9	2.024(9)	Ta7–O3	2.041(8)	Ni1–O2	2.102(9)
Ta3–O10	1.974(8)	Ta7–O6	1.954(9)	Ni1–O4	2.071(9)
Ta3–O16	1.801(9)	Ta7–O15	1.784(9)	Ni1–O5	2.074(9)
Ta4–O4	1.997(9)	Ta8–O2	2.076(9)	Ni2–O1	2.161(10)
Ta4–O11	2.005(10)	Ta8–O11	1.944(10)	Ni2–O2	2.132(9)
Ta4–O12	1.980(9)	Ta8–O22	1.801(9)	Ni2–O3	2.039(9)
Ta4–O18	1.783(9)	Ta8–O24	2.383(8)	Ni2–O28	2.045(10)

Table S6. Bond valence sum calculations of the Ta and Ni atoms in **2a**.

Atom	BVS	Atom	BVS	Atom	BVS	Atom	BVS
Ta1	5.01	Ta4	5.05	Ta7	5.02	Ta10	5.15
Ta2	4.98	Ta5	4.85	Ta8	4.99	Ni1	2.01
Ta3	4.88	Ta6	4.84	Ta9	5.03	Ni2	2.07

Table S7. Bond valence sum calculations of the oxygen atoms of **2a**

Atom	BVS	Atom	BVS	Atom	BVS	Atom	BVS
O1	1.89	O9	1.77	O17	1.36	O25	1.48
O2	1.92	O10	1.69	O18	1.49	O27	1.68
O3	1.81	O11	1.73	O19	1.36	O28	1.84
O4	1.95	O12	1.69	O20	1.41	O29	1.73
O5	1.93	O13	1.71	O21	1.42	O30	1.76
O6	1.69	O14	1.75	O22	1.38	O31	1.70
O7	1.73	O15	1.44	O23	1.31	O32	1.71
O8	1.72	O16	1.38	O24	1.82	O33	1.82

Tables S8. Assignment of mass spectral data for compound **1**

Peaks Assignment	Cal. *m/z*	Exp. *m/z*
$[H_3Na_2Ni(H_2O)_2NiTa_{10}O_{30}(OH)_2(H_2O)_5]^{3-}$	871.42	871.44
$[H_2Na_3Ni(H_2O)_2NiTa_{10}O_{30}(OH)_2(H_2O)_5]^{3-}$	878.75	878.72
$[H_2Na_3Ni(H_2O)_2NiTa_{10}O_{30}(OH)_2(H_2O)_6]^{3-}$	884.79	884.80
$[H_2Na_4Ni(H_2O)_2NiTa_{10}O_{30}(OH)_2(H_2O)_9]^{3-}$	910.10	910.12

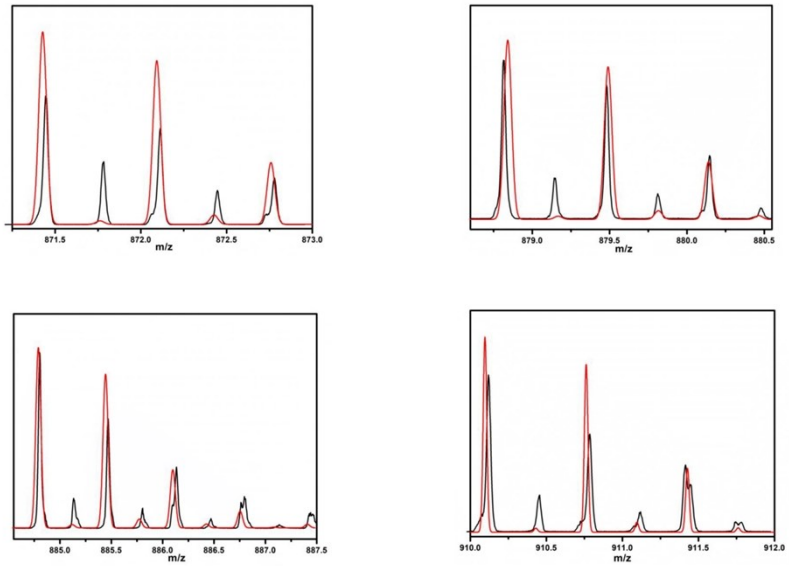

Simulated (red) and experimental (black) negative-mode mass spectra of isotopic envelopes for **1**.

Tables S9. Assignment of mass spectral data for compound **2**

Peaks Assignment	Cal. *m/z*	Exp. *m/z*
$[H_3Na_4Ni(en)NiTa_{10}O_{32}(H_2O)_3]^{3-}$	882.09	882.08
$[H_2Na_5Ni(en)NiTa_{10}O_{32}(H_2O)_6]^{3-}$	907.41	907.39
$[K_2Na_5Ni(en)NiTa_{10}O_{32}(H_2O)_3]^{3-}$	914.71	914.73
$[KNa_6Ni(en)NiTa_{10}O_{32}(H_2O)_5]^{3-}$	921.41	921.39
$[K_2Na_5Ni(en)NiTa_{10}O_{32}(H_2O)_5]^{3-}$	926.72	926.73
$[H_2K_5Ni(en)NiTa_{10}O_{32}(H_2O)_{10}]^{3-}$	958.73	958.70

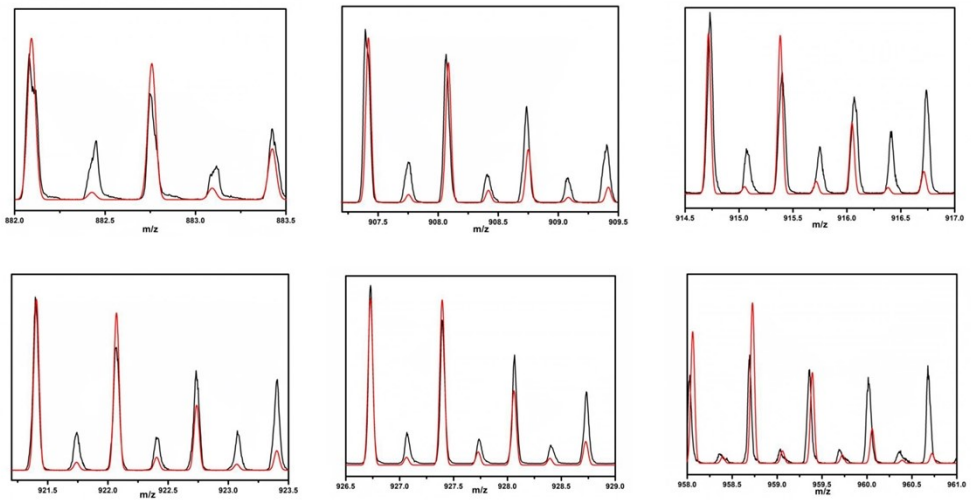

Simulated (red) and experimental (black) negative-mode mass spectra of isotopic envelopes for **2**.

Table S10. Catalytic performance of different factors in the transesterification reaction[a]

Entry	Catalyst (μmol)	(DMC: EtOH) (ml)	Temperature (°C)	Time (h)	Yield (%)
1	0.4	1:4	100	2	47.2
2	0.8	1:4	100	2	52.1
2	1	1:4	100	2	60.2
3	1.2	1:4	100	2	58.3
4	1.6	1:4	100	2	57.2
5	1	1:4	80	2	23.2
6	1	1:4	120	2	51.4
7	1	1:4	100	1	46.5
8	1	1:4	100	3	57.8

[a]Reaction conditions: catalyst (1μmol), DMC (6mmol), CH_2CH_3OH (34 mmol, 2 mL), 100°C, 2h. The products were qualitatively analyzed by GC−MS and quantitatively analyzed by GC.

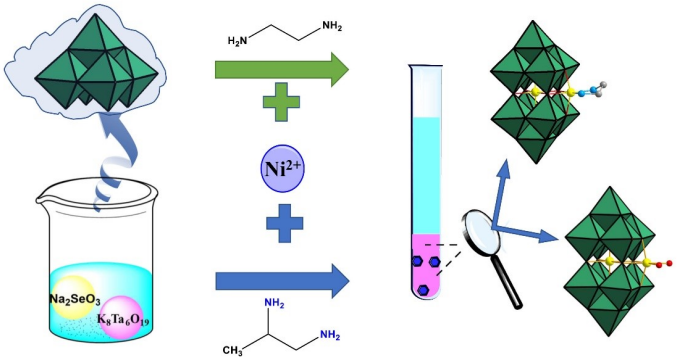

Figure S1. The preparation process of **1** and **2**.

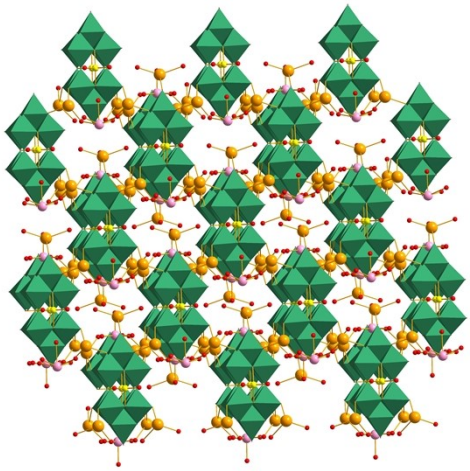

Figure S2. the 3D framework of **1**. (Ta: green; Ni: yellow; O: red; K: orange; Na: rose)

Section 3 Additional measurements

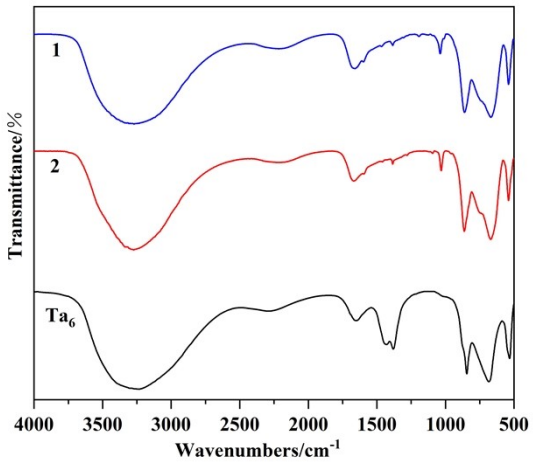

Figure S3. The IR spectra of **1**, **2** and **Ta_6**.

The IR spectra of **1**, **2**, and **Ta_6** were recorded between 4000 and 500 cm^{-1}. The absorption peaks at 857, 735, 670, and 538 cm^{-1} for **1**, 863, 746, 675, and 539 cm^{-1} for **2** can be ascribed to terminal Ta=O_t and the bridging Ta–O_b–Ta vibrations.[3] The Ta–O_b–Ta vibration bands of **1** and **2** split into more components, due to the {Ni(en)Ni} or {Ni_2} unit grafting onto {Ta_6O_{19}} cluster by comparison with **Ta_6**.[4,5] The vibration of en ligand has a range of 1017–1044 cm^{-1} in **2**.[6] The wide peaks at 3500–3250 cm^{-1} for **1** and **2** are attributed to bending and stretching modes of the water molecules.

Compounds	v (Ta=O_t)	v (Ta-O_b-Ta)
1	857 cm^{-1}	735, 670, 538 cm^{-1}
2	863 cm^{-1}	764, 675, 539 cm^{-1}

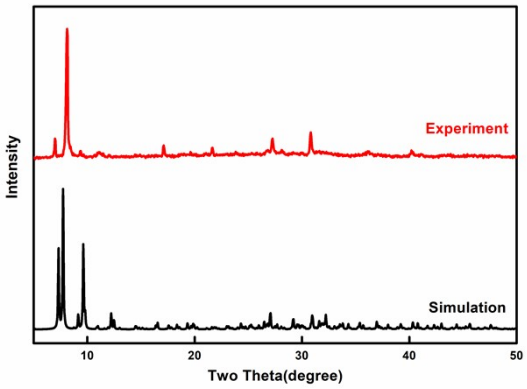

Figure S4. The simulated and experimental PXRD patterns of **1**

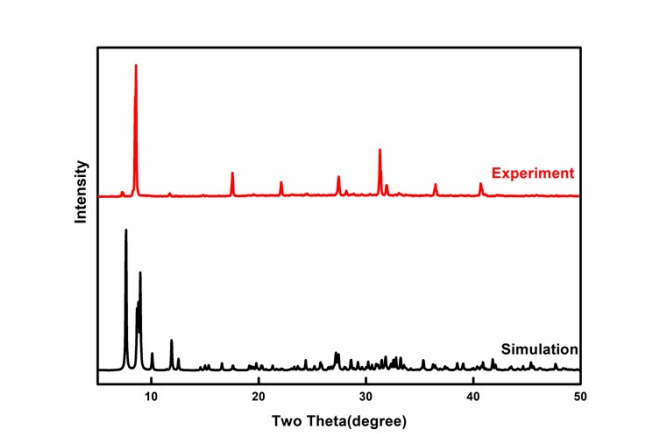

Figure S5. The simulated and experimental PXRD patterns of **2**

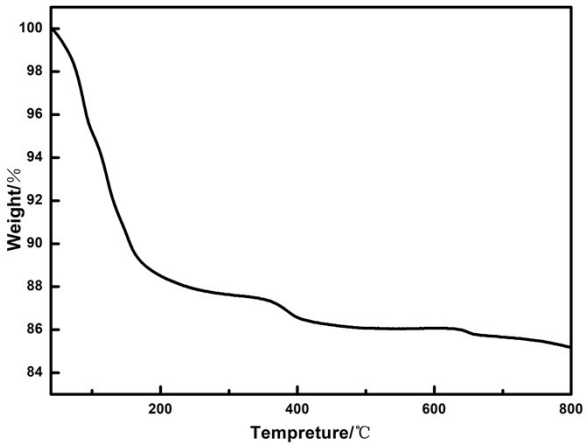

Figure S6. The TGA curve of **1**.

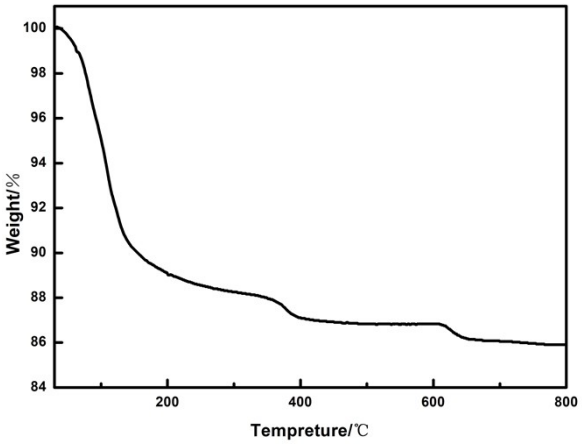

Figure S7. The TGA curve of **2**.

At a temperature range of 1.8–300 K, the magnetic susceptibilities of compounds **1** and **2** have been studied in a 1000 Oe magnetic field. For **1**, the value of χ_MT increased from 5.04 emu K mol^{-1} at 300 K to 6.67 emu K mol^{-1} at 7.7 K, which shows the presence of ferromagnetic couplings between Ni^{2+} ions. The χ_MT products drop dramatically below 7.7 K, which might be caused by zero-field splitting.[7] The curve fitting for χ_M^{-1} versus T polts obeys the Curive-Weiss law, with C = 5.0 emu K mol^{-1} and θ =2.99 K (Figures S8 and S9) and it further shows that the presence of the ferromagnetic couplings between Ni^{2+} centers.[8,9] The value of χ_MT is 5.04 emu K mol^{-1} at 300 K, this is apparently beyond the theoretical value of 2 emu K mol^{-1} for 2 non-interacting Ni^{2+} ions (S =1, g =2.0), on account of the spin-orbit interaction and ferromagnetic coupling.[10] For **2**, with the temperature dropped in the range of 300–10 K, the χ_MT value increased from 2.62 emu K mol^{-1}to 3.30 emu K mol^{-1} (Figures S10 and S11). Under 10 K, the χ_MT value decreased sharply, which was also attributed to zero-field splitting effect. The curve fitting for χ_M^{-1} versus T polts obeys the Curive-Weiss law, with C = 2.70 emu K mol^{-1} and θ =2.16 K, which manifests that the presence of the ferromagnetic couplings between Ni^{2+} ions in compound **2**.

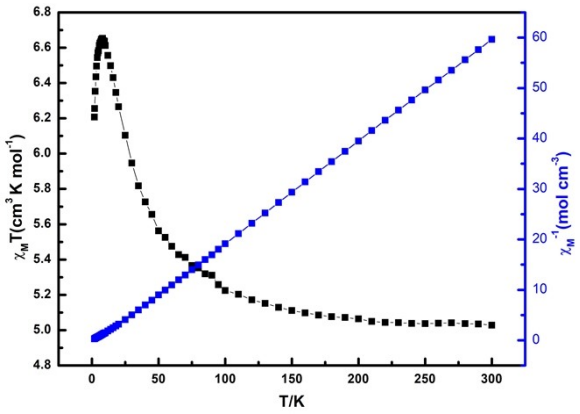

Figure S8. Temperature dependence of $\chi_M T$ between 1.8 and 300 K and χ_M^{-1} for compound **1**.

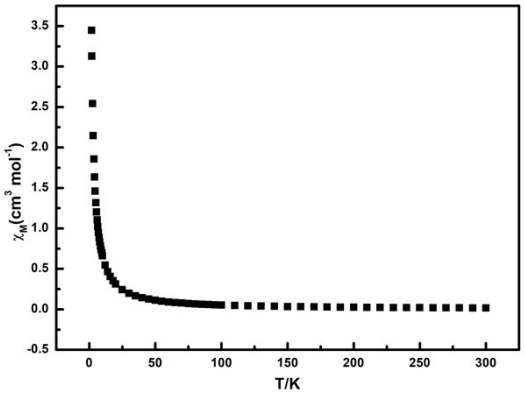

Figure S9. Temperature dependence of the molar magnetic susceptibility χ_M for **1** between 1.8 and 300 K.

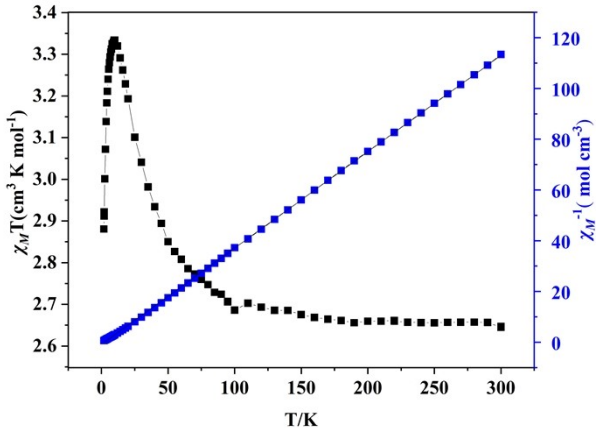

Figure S10. Temperature dependence of χ_MT and χ_M^{-1} between 1.8 and 300 K for **2**

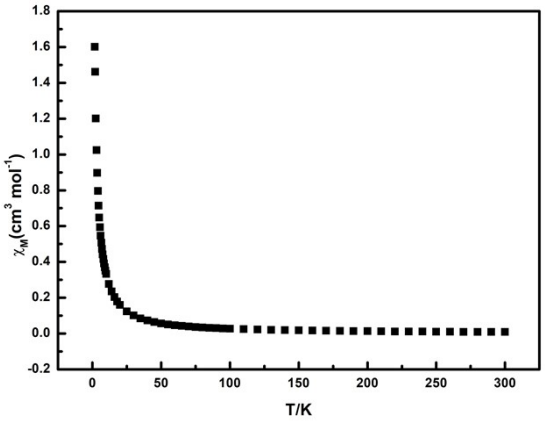

Figure S11. Temperature dependence of the molar magnetic susceptibility χ_M for **2** between 1.8 and 300 K.

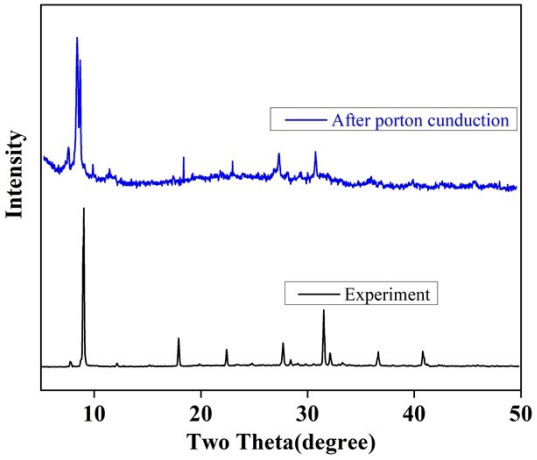

Figure S12. The powder X-ray diffraction measurement patterns of **2**.

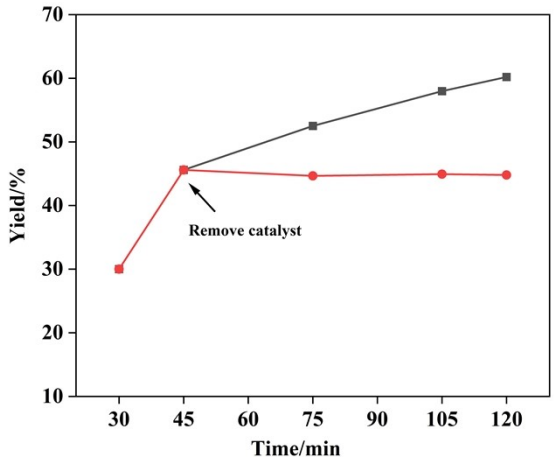

Figure S13. Hot filtration test for catalyst.

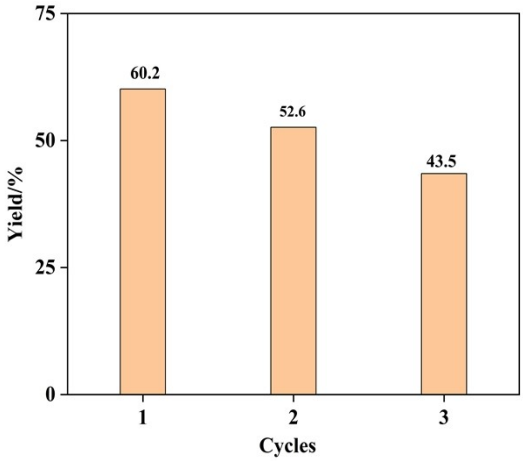

Figure S14. Recyclability of catalyst. (The yields gradually decreased to 60.2%, 52.6%, and 43.5% due to the catalyst loss during the washing process and some active sites were covered by substrates)

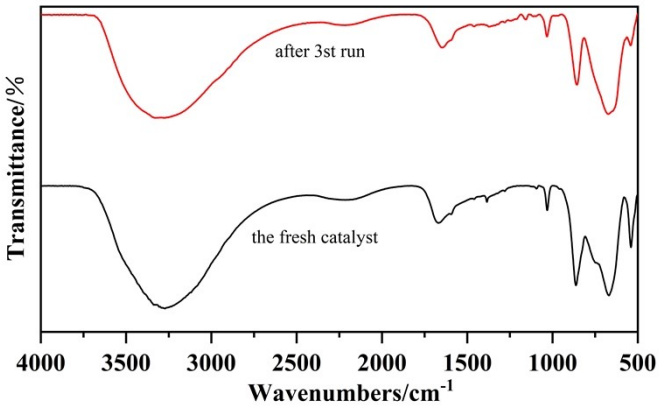

Figure S15. IR spectra of **2** after reaction.

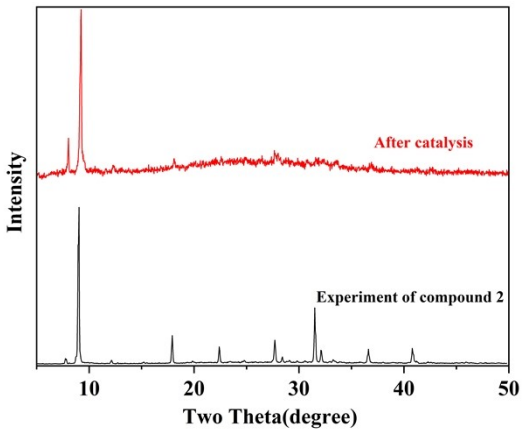

Figure S16. PXRD spectra of **2** after reaction.

Section 4 References

1 Filowitz, M., Ho, R. K. C., Klemperer, W. G and Shum, W. *Inorg. Chem*. 1979, **18**, 93–103.
2 G. M. Sheldrick, *Acta Cryst.*, 2008, **A64**, 112–122.
3 G.-L. Guo, Y.-Q. Xu, B.-K. Chen, Z.-G. Lin and C.-W. Hu, *Inorg Chem Commun.*, 2011, **14**, 1448–1451.
4 Y. Ma, J. Sun, C. Li, N. Li, P. Ma, D. Zhang, G. Wang and J. Niu, *Inorg Chem Commun.*, 2019, **101**, 6–10.
5 S. Li, S. Chen, F. Zhang, Z. Li, C. Zhang, G. Cao and B. Zhai, *Inorg Chem Commun.*, 2019, **106**, 228–232.
6 L. Li, Y. Niu, K. Dong, P. Ma, C. Zhang, J. Niu and J. Wang, *RSC Adv.*, 2017, **7**, 28696–28701.
7 Z. Liang, D. Zhang, H. Wang, P. Ma, Z. Yang, J. Niu and J. Wang, *Dalton Trans.*, 2016, **45**, 16173–16176.
8 Y. Hou, L. Xu, M. J. Cichon, S. Lense, K. I. Hardcastle and C. L. Hill, *Inorg. Chem.*, 2010, **49**, 4125–4132.
9 A. P. Ginsberg, J. A. Bertrand, R. I. Kaplan, C. E. Kirkwood, R. L. Martin and R. C. Sherwood, *Inorg. Chem.*, 1971, **10**, 240–246.
10 I. M. Mbomekalle, B. Keita, M. Nierlich, U. Kortz, P. Berthet and L. Nadjo, *Inorg. Chem.*, 2003, **42**, 5143–5152.